

Cite this: DOI: 10.1039/c0xx00000x

www.rsc.org/xxxxxx

ARTICLE TYPE

Imaging the photodissociation dynamics of neutral metal clusters: Copper dimer, Cu₂, and copper oxide, CuO

Imogen S. Parry, Alexander C. Hermes, Aras Kartouzian and Stuart R. Mackenzie*

Received (in XXX, XXX) Xth XXXXXXXXX 20XX, Accepted Xth XXXXXXXXX 20XX

DOI: 10.1039/b000000x

The spectroscopy and UV photodissociation dynamics of Cu₂ and CuO have been studied using a combination of one- and two-colour excitation and velocity map imaging. Resonant excitation of Cu₂ via the $J \leftarrow X^1\Sigma_g^+$ transition leads to significant fragmentation which is interpreted in terms of a combination of direct dissociation of Cu₂⁺ $^2\Pi$ produced in the resonant two-photon ionization process and dissociation of excited Cu₂ states above the ionization threshold. By fitting of the kinetic energy release spectra obtained from the velocity map images, we determine a value for the dissociation energy of the cation of D_0 (Cu₂⁺, $X^2\Sigma_g^+$) of 1.713 ± 0.025 eV, which, when combined with known ionization energies, yields D_0 (Cu₂, $X^1\Sigma_g^+$) = 1.886 ± 0.026 eV. In other experiments, resonant two colour (1+1') excitation of CuO via a range of excited states (*C*, *D*, *F*, *H*), yields unusually simple VMI images indicating fragmentation into a single dissociation channel which has been identified as Cu* $^2D_{3/2}$ + O* 1D . Taken together, this data gives a CuO bond dissociation energy of 3.041 ± 0.030 eV. Finally, the production of Cu₂⁺ with kinetic energy = 705 ± 75 cm⁻¹ is tentatively interpreted as photolysis of Cu₃ yielding Cu* + Cu₂ $X^1\Sigma_g^+$ from which a dissociation energy of Cu₃ of 0.605 ± 0.030 eV is deduced.

1. Introduction

The electronic structures of small metal and metal-containing molecules and clusters have been studied in detail ever since the development of pulsed laser ablation cluster sources rendered the isolated species amenable to techniques such as laser induced fluorescence and photoionization.^{1, 2} This activity stems, in part, from a desire to better understand the fundamentals of bonding in metals and also from a need to explore key interactions relevant in heterogeneous catalysis.

The coinage metal dimers have long been favourites for study. Their simple ground states, with closed *d*-shells, and open *d*-shell excited states has made them something of a benchmark system for both experimental^{1, 3-5} and computational approaches.⁶⁻⁹ Small isolated copper clusters, including the dimer, were first studied spectroscopically in the early 1980s by the Smalley group¹⁰⁻¹³ and others.¹⁴ Since then the isolated dimer alone has been studied by techniques such as fluorescence,¹⁴⁻¹⁶ direct absorption,¹⁷ FT emission,¹⁸ photoionization spectroscopy,¹⁹⁻²¹ and collision induced dissociation (CID) techniques.^{22, 23} Computationally, Miyoshi *et al.* performed a series of high quality *ab initio* calculations on Cu₂²⁴ and developments since have been reviewed recently by Lecoultré *et al.* in their time-dependent density functional theory study.²⁵ As well as the fundamental interest, Cu₂ embedded within proteins has also been implicated recently in the biological oxidation of methane.²⁶

Transition metal oxides play important roles in processes such as corrosion, heterogeneous catalysis, astrophysics and biology. Accordingly, their spectroscopy has been well-studied and reviewed.²⁷⁻²⁹ Appelblad *et al.* have characterised a variety of

visible bands by laser induced fluorescence³⁰ and a useful summary of these and other findings was reported by Schamps *et al.*³¹ More recently CuO has been the subject of several high resolution studies to determine properties such as the electric dipole moment,³² magnetic and nuclear hyperfine parameters.^{33, 34} It has also been the subject of several anion photoelectron spectroscopy studies.^{35, 36} Theoretical approaches to CuO have been reviewed recently²⁹ and this is a system in which density functional theory has had notable successes.^{37, 38}

Recently, we have developed a velocity map imaging (VMI)³⁹ instrument equipped with laser ablation metal cluster source for the purpose of studying the photodissociation dynamics of small metal and metal-containing clusters. In particular we are interested in the study of neutral clusters which pose particular problems for VMI study. In such studies, no mass selectivity is possible and the size and composition distribution within the cluster beam is different for every instrument and, in general, unknown. Photoionization is commonly used to characterise the size distribution of neutral cluster beams. However, this requires near threshold ionization to prevent fragmentation of the cations.⁴¹ The ionization energies of small transition metal clusters typically exhibit large size dependence making this method potentially unreliable. Copper is a good example of this with vertical ionization energies (IEs) of small Cu_{*n*} clusters changing dramatically between adjacent cluster sizes, especially in the range *n* = 1-20.⁴² The IEs also exhibit marked odd-even variations and regular maxima and minima characteristic of electronic shell models which is seen in other clusters including Ag_{*n*}.⁴³ This lack of size-selectivity in the cluster beam means that

it can be

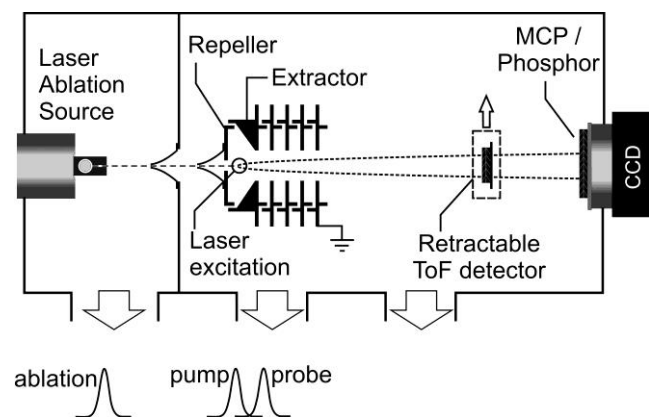


Fig. 1 Velocity map imaging spectrometer complete with pulsed laser ablation metal cluster source. The time-of-flight detector is withdrawn for imaging studies. The delay between ablation and probe pulse is *ca.* 90 μ s. For two-colour studies, the visible (pump) probe fires typically 30ns before the (UV) probe to permit discrimination of one- and two-colour processes in time of flight.

challenging to assign a dissociation process resulting in a fragment X to a particular species since neither the dissociation energy nor the quantum state (or even the identity) of the co-fragment are typically known. Typically a spectroscopic signature of the molecular carrier is required and in this manner we have previously succeeded in studying the VUV dissociation of Au_2 ,⁴⁴ the UV dissociation of Au-RG (RG = Ar, Kr, Xe)^{45, 46} and Xe_2 complexes^{47, 48} and the IR photofragmentation of $\text{Li}(\text{NH}_3)_4$.⁴⁹

Here, we apply similar VMI techniques to Cu_n ($n = 2, 3$) and CuO in which a combination of electronic spectroscopy and photofragment imaging is used to unravel the fragmentation dynamics and deduce parent molecule dissociation energies.

2. Experimental

Fig. 1 shows a schematic of the instrument used in these studies. It comprises a conventional velocity map imaging (VMI) spectrometer equipped with pulsed laser ablation metal cluster source and the salient points have been described in detail previously.^{44, 45, 47} In previous studies the mass resolving power of the instrument had been limited by the use of the imaging MCP phosphor assembly in time-of-flight (ToF) mode. To rectify this and extend the lifetime of the imaging plates, a second retractable ToF detector has recently been installed for spectroscopic studies (see Fig. 1). In a second change to the experiment, we have replaced the solenoid valve previously used with a Jordan valve. By virtue of its shorter pulse duration this permits higher backing pressures to be used and can result in more efficient clustering. The image acquisition and analysis protocols remain unchanged from previous studies.^{44, 45} No attempts at slice imaging were made, typical cluster signals in previous studies having proved too low. Signal levels recorded here, however, were markedly higher and such an approach may prove beneficial in future. The conical extractor design, coupled with step-down dynode chain results in a more homogeneous field in the VMI region compared with a traditional three electrode arrangement by reducing field penetration.⁵⁰ This offers

advantages in detecting low kinetic energy release processes and results in an effective magnification factor of 1.07 as determined by a combination of ion trajectory simulations and earlier calibration studies.

Copper-containing molecules and/or clusters were produced by laser ablation of a rotating copper foil target in the presence of a helium carrier gas seeded with 5–10% nitrous oxide (BOC) admitted from a backing pressure of 4 bar. The N_2O served to increase the number density of oxides in the beam but was also observed to enhance the Cu_2 production over a pure helium backing gas.

By virtue of the static potentials applied to the VMI electrodes, only neutral species make it into the spectroscopy region of the instrument. Here, the molecular beam is intersected orthogonally by the output of a frequency doubled dye-laser (UV probe, Sirah Cobra Stretch, < 2 mJ per 10 ns pulse) operated in the region $260 \text{ nm} < \lambda < 280 \text{ nm}$. In the majority of studies reported here, this UV probe pulse was fixed to be resonant at the one-photon level with the $J(v=0) \leftarrow X(v=0)$ transition in $^{63}\text{Cu}_2$ (previously Smalley's "system V")¹¹ at 267.06 nm.^{1, 21} In two-colour experiments, especially in the study of CuO, a second pump pulse, comprising the signal output of a 355 nm pumped optical parametric oscillator (Continuum Panther) is arranged to co-propagate with the UV beam and fires typically 30 ns before the probe. This delay is sufficient to permit resolution of visible only and true two-colour processes in the time-of-flight spectrum which proved useful in simplifying the analysis. Both lasers are weakly focused into the cluster beam with a common 30 cm focal length lens.

3. Results and Discussion

3.1 Cu_2^+ UV photoionization and photodissociation

The upper part of Fig 2 shows the spectrum recorded in the $^{63}\text{Cu}_2^+$ and $^{63}\text{Cu}^+$ mass channels as the UV laser is scanned in the region of the $J(v=0) \leftarrow X^1\Sigma_g^+(v=0)$ transition around 267 nm. The Cu_2^+ spectrum was first reported by Powers *et al.* at low resolution and labelled "system V".¹¹ It has since been characterised by rotationally resolved fluorescence excitation spectroscopy although due to heavy perturbation in the spectrum the symmetry of the J state remains to be determined.¹⁵ In the Cu_2^+ channel, signal arises from the straightforward resonant two-photon ionization (R2PI) process. This process has been studied in detail by Sappey *et al.* using photoelectron spectroscopy (PES).^{20, 21}

The Cu_2^+ spectrum is mirrored approximately in the Cu^+ channel indicating a significant degree of photofragmentation. By way of investigating the likely fragmentation mechanism(s) involved we have recorded one-colour VMI images at this wavelength and the resulting total kinetic energy release (TKER) spectrum is shown in the lower portion of the Fig 2.

1+1 ionization of Cu_2 via the $J(v=0)$ state produces both ground $X^2\Sigma_g^+$ and excited $^2\Pi$ states of Cu_2^+ in a ratio of around 3:1.²¹ Ionization to the $^2\Pi$ states ($^2\Pi_{3/2}$ at $9219 \pm 11 \text{ cm}^{-1}$ and $^2\Pi_{1/2}$ at $10127 \pm 16 \text{ cm}^{-1}$ above the $X^2\Sigma_g^+$) is a direct process and the relative intensities of vibrational bands in the PES spectrum are well-modelled by Franck-Condon simulations.²¹ By contrast, ionization to the $\text{Cu}_2^+ X^2\Sigma_g^+$ ground state leads to extraordinary

vibrational excitation in the cation with levels $0 \leq v^+ \leq 49$ excited.

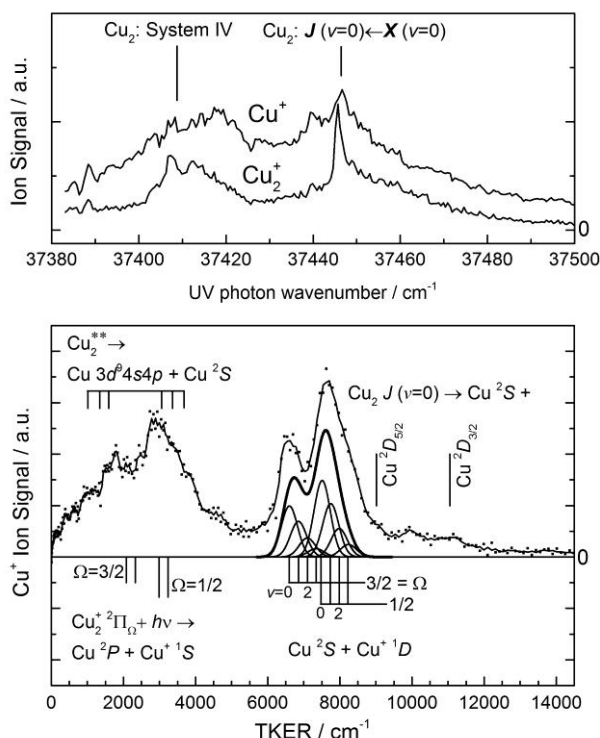
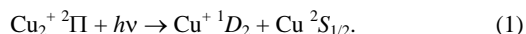


Fig 2 (upper) UV R2PI spectrum recorded in the $^{63}\text{Cu}_2^+$ and $^{63}\text{Cu}^+$ channels simultaneously. (lower) Total kinetic energy release (TKER) spectrum determined from the velocity map image of $^{63}\text{Cu}^+$ fragments following excitation of the $\text{Cu}_2 J(v=0) \leftarrow X^1\Sigma_g^+(v=0)$ transition at 37446 cm^{-1} . Assignments marked below the spectrum correspond to one-photon dissociation of the $\text{Cu}_2^+ {}^2\Pi$ state, those marked above to dissociation on the neutral surface at either the one or two photon level.

This long progression was interpreted by Sappey *et al.* as evidence for dissociative autoionization of doubly excited Cu_2^{**} states above the Cu_2 ionization threshold. If the dissociation competes with ionization, this would lead to significant bond-length extension and could, therefore, account for the extensive vibrational progression observed.

The TKER spectrum extracted from the velocity map image of the Cu^+ (Fig 2) recorded at the peak of the $\text{Cu}_2^+ J \leftarrow X$ band head at 37446 cm^{-1} exhibits a broad, largely unresolved feature at $\text{TKER} < 5000 \text{ cm}^{-1}$ and an apparent doublet feature at $6000 < \text{TKER}/\text{cm}^{-1} < 9000$. The separation of the peaks in the doublet matches approximately the spin-orbit splitting in the $\text{Cu}_2^+ {}^2\Pi$ state (909 cm^{-1}) and we tentatively assign these features to the one-photon dissociation of the cation:



The exact TKER for this process depends on the Cu_2^+ dissociation energy for which a variety of values have been reported. Sappey *et al.* used their measured Cu_2 ionization energy ($7.899 \pm 0.007 \text{ eV}$) and a $2.01 \pm 0.08 \text{ eV}$ dissociation energy for ground state Cu_2 to deduce a value for $D_0(\text{Cu}_2^+, X^1\Sigma_g^+)$ of $1.84 \pm 0.08 \text{ eV}$.²¹ More recently, Ingólfsson *et al.* reported a value of $1.64 \pm 0.14 \text{ eV}$ from energy resolved collision induced dissociation studies and Krückeberg *et al.* similarly determined a

value of $1.57 \pm 0.08 \text{ eV}$. Under the assumption that the intense doublet in the TKER spectrum arises from the photodissociation channel (1) the best fit to the VMI data is provided by assuming $D_0(\text{Cu}_2^+, X^1\Sigma_g^+)$ of $1.713 \pm 0.025 \text{ eV}$. The simulations shown in Fig 2 for these features include the relative vibrational branching ratios of $\text{Cu}_2^+ {}^2\Pi$ levels observed in the PES spectrum ($v = 0, 1, 2, 3$).²¹ Excitation out of these various vibronic levels accounts for the width of the TKER features. One difference with the Sappey *et al.* results is marked. In the R2PI PES spectrum, the $\text{Cu}_2^+ {}^2\Pi_{3/2} : {}^2\Pi_{1/2}$ branching ratio was around 3 for ionization out of the $J(v=0)$ level. By contrast, if our assignment is correct, we observe approximately 50% more fragmentation products from the upper (${}^2\Pi_{1/2}$) spin-orbit component. These results are not necessarily inconsistent but would indicate a much stronger photodissociation cross-section out of the ${}^2\Pi_{1/2}$ state.

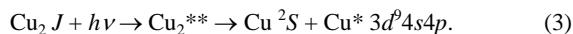
The ionization energies of both Cu (7.726 eV)⁵¹ and Cu_2 (7.899 eV)²¹ are well known and thus from the above D_0 for Cu_2^+ we can determine the neutral Cu_2 experimental dissociation energy of $1.886 \pm 0.026 \text{ eV}$. This is slightly lower than the $16760 \pm 200 \text{ cm}^{-1}$ ($2.078 \pm 0.025 \text{ eV}$) value Rohlfing and Valentini determined for D_e from a Birge-Sponer extrapolation of their vibrationally resolved dispersed fluorescence data¹⁶ but closer to the $185.7 \pm 2.8 \text{ kJ mol}^{-1}$ ($1.925 \pm 0.029 \text{ eV}$) atomization enthalpy of Hilpert and Gingerich from variable temperature mass spectrometry.⁵² By virtue of the agreement on the $D_0(\text{Cu}_2^+, X^1\Sigma_g^+)$, our value is, necessarily, consistent with the $1.81 \pm 0.14 \text{ eV}$ determined by Ingólfsson for $D_0(\text{Cu}_2)$.

We cannot rule out a contribution to the TKER spectrum from dissociation of the $\text{Cu}_2 J$ state but the possibilities are limited, with only the following dissociation channels lying in this TKER range:



These thresholds are marked on Fig 2 assuming the Cu_2 dissociation energy determined above.

The other major feature in the TKER spectrum is the unresolved feature below 5000 cm^{-1} . We assign signal in this region to Cu_2^{**} dissociation (*i.e.*, on the neutral surface at the 1+1 photon level) yielding highly excited state copper atoms:



Besides the energetic match, there is independent evidence for such an assignment. Sappey *et al.* noted peaks in their photoelectron spectrum which they tentatively attributed to ionization of $\text{Cu}^* 3d^9 4s4p$ states lying $>6 \text{ eV}$ above the Cu ground state in support of their dissociative autoionization mechanism.²¹ Signal in the TKER region $1000 - 3700 \text{ cm}^{-1}$ is consistent with generation of the ${}^2F^\circ$, ${}^2P^\circ$ and ${}^2D^\circ$ terms arising from this configuration.⁵³ Other, lower-lying terms would result in higher kinetic energy fragments outside the detected TKER range.

Analysis of the one colour VMI data (including *via* other intermediate states) continues in our group but in the two-colour experiments upon which the remainder of the current paper concentrates, the UV-only signal represents a background contribution which can be reliably subtracted to yield the true two-colour contribution.

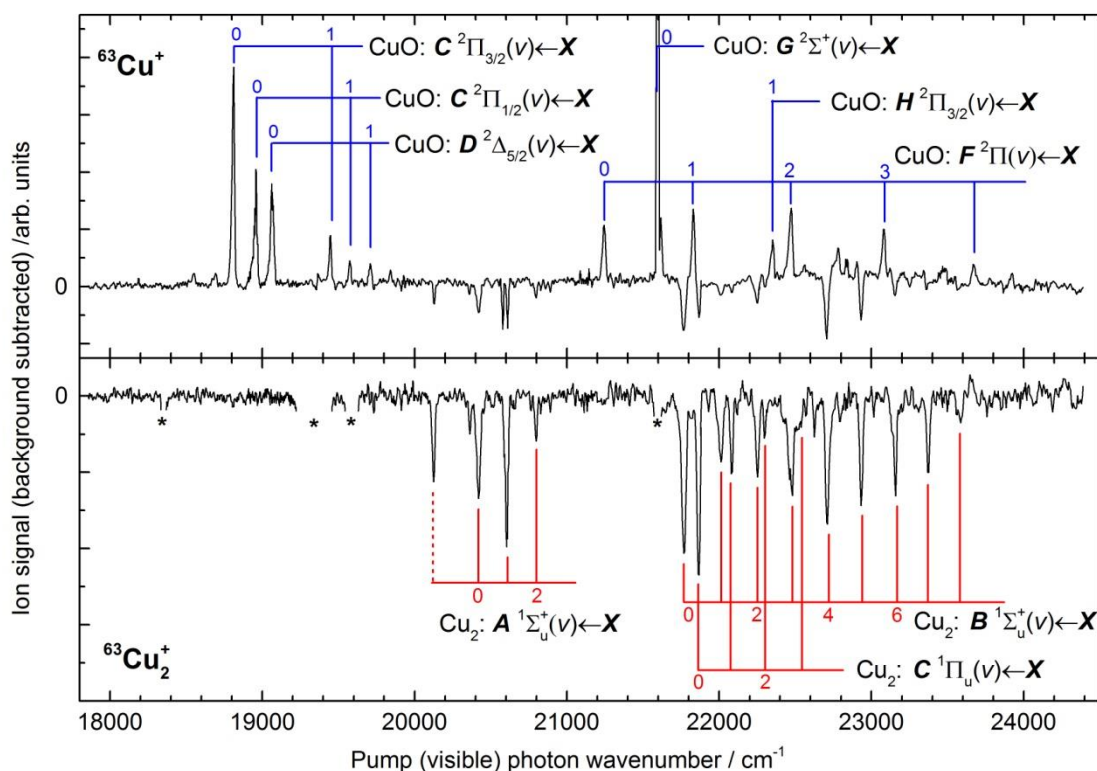


Fig. 3 (colour online) Overview spectrum of two-colour enhancements and depletions recorded in the $^{63}\text{Cu}^+$ (upper) and $^{63}\text{Cu}_2^+$ (lower) mass channels as a function of (visible) pump laser wavenumber. Both upper and lower traces have been background corrected for the one-colour signal arising from the UV laser set resonant with the $^{63}\text{Cu}_2 J(v=0) \leftarrow X(v=0)$ transition at 37446 cm^{-1} . Asterisks mark the positions of artefacts arising from intense atomic transitions (removed for clarity).

3.2 Two-colour spectroscopy

Fig 3 shows the two-colour spectra recorded in the $^{63}\text{Cu}_2^+$ and $^{63}\text{Cu}^+$ mass channels as the visible pump beam is scanned from 550 nm to 410 nm with the UV probe fixed to be on resonance with the $\text{Cu}_2 J(v=0) \leftarrow X^1\Sigma_g^+(v=0)$ band (henceforth labelled with a prime). The spectra in both mass channels have been background corrected for the UV-only contributions discussed above.

The two-colour spectrum in the Cu_2^+ channel exhibits clear dips arising from depletion of the $\text{Cu}_2 X(v=0)$ level when the visible beam is resonant with transitions to the low-lying $\text{Cu}_2 A^1\Sigma_u^+$, $B^1\Sigma_u^+$ and $C^1\Pi_u$ electronic states.¹ These states have all been well characterised by fluorescence excitation spectroscopy¹⁵ and all transitions can be confidently assigned on this basis.⁵⁴

The same dips observed in the two-colour Cu_2^+ spectra are also observed in the Cu^+ mass channel (see Fig 3) reflecting the fact that the background signal originates either directly from, or as transitions out of, the $\text{Cu}_2 J$ state (see Fig 4).

The Cu^+ spectrum also exhibits intense enhancements which can be assigned (see below) to altogether different processes originating in the CuO molecule. These transitions are not observed in either the Cu_2^+ or indeed the CuO^+ channel and highlight a challenging feature of studying neutral clusters and molecules where mass-selectivity is impossible. Despite adding

N_2O to the backing line specifically to generate Cu_nO_m species, no oxides are observed in the mass spectrum following UV excitation even when ionizing with a 157 nm (7.9 eV) F_2 excimer laser pulse, the IE of CuO having been determined to be $9.41 \pm 0.01\text{ eV}$.⁵⁵

3.2.1 ^{63}CuO Spectroscopy

In amongst the dips arising from the Cu_2 transitions, a number of strong spectral enhancements are observed in the Cu^+ channel in the region $21\,000 - 24\,000\text{ cm}^{-1}$ the intense bands of which are assigned on Fig 3 on the basis of previous fluorescence studies.^{30, 56, 57} Clear features observed include a strong progression in the $\text{CuO } F^2\Pi_i \leftarrow X^2\Pi_{3/2}$ transition. Given the linewidth of our OPO pump laser ($\sim 5\text{ cm}^{-1}$) we cannot observe rotational structure but given that Appelblad and Lagerqvist only observed $\Delta\Omega = 0$ transitions in the fluorescence spectrum it is likely that it is the $F^2\Pi_{3/2}$ state which is excited. Other intense peaks in this region may be ascribed to the $G^2\Sigma$ origin band and the $H^2\Pi_{3/2}(v=1) \leftarrow X^2\Pi_{3/2}(v=0)$ band (the 0-0 band on this transition never having been observed).⁵⁸ Additional, weaker features in the spectrum match transitions to a range of additional electronic states including the $k^4\Sigma_{1/2}$ state (22818 cm^{-1}) but again the spectral linewidth of the pump laser employed here prohibits their rotational resolution.

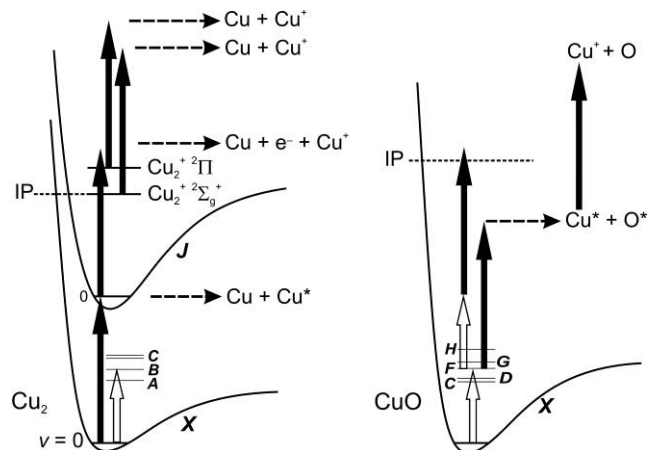


Fig. 4 Schematic electronic states of Cu_2 (left) and CuO (right) involved in the observed one- and two-colour spectroscopy and/or dissociation dynamics (see text for details). Relative energies are shown approximately to scale. Full arrows represent UV (probe) photons and open arrows visible (pump) photons. In two-colour experiments the pump pulse fires up to 50 ns before the UV probe.

In the spectral region $18500 - 20000 \text{ cm}^{-1}$, a further three short progressions are observed which can be assigned as $\text{CuO } C^2\Pi_{3/2, 1/2}(v) \leftarrow X^2\Pi_{3/2}(v=0)$ and $D^2\Delta_{5/2}(v) \leftarrow X^2\Pi_{3/2}(v=0)$ transitions.⁵⁹ Very weak features around 270 cm^{-1} to the red of the $C^2\Pi_{3/2, 1/2}(v) \leftarrow X^2\Pi_{3/2}(v=0)$ bands, respectively, are almost certainly the equivalent transitions out of the upper, $X^2\Pi_{1/2}$, spin-orbit component of the ground state, which, lying 277 cm^{-1} higher than the $^2\Pi_{3/2}$ level, is only weakly populated in the molecular beam. The $D^2\Delta_{3/2}(v=0) \leftarrow X^2\Pi_{3/2}(v=0)$ transition is probably obscured by the $C^2\Pi_{1/2}(v=0) \leftarrow X^2\Pi_{3/2}(v=0)$ band around 18950 cm^{-1} .

All of the above spectral features observed can be satisfactorily assigned to CuO transitions on the basis of their spectral positions. However, it is far from clear how excitation in this spectral region generates the Cu^+ signal detected given that all of the excited states assigned lie below the CuO ground state dissociation energy, which guided ion beam studies have previously placed at $2.94 \pm 0.12 \text{ eV}$ (*ca.* $23713 \pm 970 \text{ cm}^{-1}$, though see below).⁶⁰ Possible routes to the production of Cu^+ following assigned transitions in CuO are illustrated on the right hand side of Fig 4. These include resonant $1+1'$ excitation resulting in fragmentation on neutral potential energy surfaces yielding electronically excited Cu^* which can be ionized by absorption of additional UV photon(s). $1+2'$ excitation would exceed the CuO ionization energy but only by $0.85 - 1.60 \text{ eV}$ which is unlikely to result in dissociation of the ion.

Fig 5 shows the two-colour Cu^+ TKER spectrum with the pump laser resonant with the $\text{CuO } F^2\Pi(v=0) \leftarrow X^2\Pi(v=0)$ at 21249 cm^{-1} and the probe (UV) laser at 37446 cm^{-1} . Under VMI focusing conditions, the temporal resolution of our instrument does not permit the separation of one- and two-colour contributions and the one-colour (UV-only) contribution discussed in Section 3.1 is clearly visible (see Fig 5a). Note that the TKER range over which it apparently extends is greater than in Fig 2 as the data is extracted under the assumption of a ^{16}O co-fragment rather than another ^{63}Cu atom. Nevertheless, as shown in Fig 5 it can easily be subtracted from the TKER spectrum to yield the two-colour contribution.

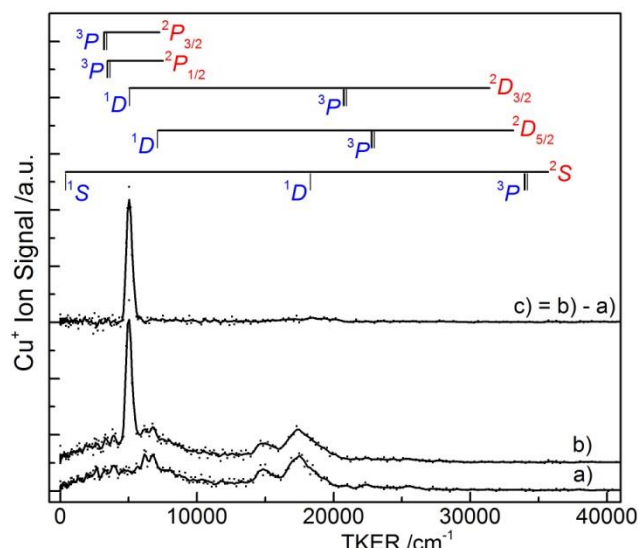
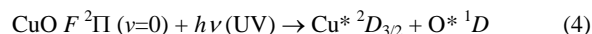


Fig. 5 (colour online) Two-colour TKER spectrum with pump laser resonant with the $\text{CuO } F^2\Pi(v=0) \leftarrow X^2\Pi(v=0)$ transition. Spectra a), b) and c) illustrate the background subtraction of the one-colour (UV only) contribution, a). The dissociation thresholds indicated (Cu atom term in red, O atom term in blue) assume a ground state $\text{CuO } D_0 = 3.041 \text{ eV}$ as determined from Fig 7 (see text for details).

Despite the large number of open dissociation continua at the $1+1'$ level ($> 4.2 \text{ eV}$ above the CuO dissociation threshold), only a single intense feature at $\text{TKER} = 5200 \text{ cm}^{-1}$ is observed in the TKER spectrum indicating a strong propensity for fragmentation into a single channel. Also marked on Fig 5 are the calculated TKER for dissociation into a range of open dissociation channels at the combined $1+1'$ level. In marking these positions, a CuO ground state dissociation energy of 3.041 eV has been assumed (see below for the determination of the CuO dissociation energy). The two-colour TKER peak represents an excellent match for dissociation into the channel



The same dissociation channel dominates UV excitation out of each vibrational level of the $\text{CuO } F$ state as illustrated in Fig 6. Shown inset in Fig 6 is the reconstructed VMI image recorded for photodissociation out of the $F(v=2)$ level. The image indicates a clear slightly parallel character to this photodissociation process. We have fit the angular distribution including up to β_4 terms. In doing so anisotropy parameters, $\beta_2 = 1.0 \pm 0.1$ and $\beta_4 = 0.0 \pm 0.2$ are determined.⁴⁰ Similar parallel anisotropy is observed for excitation out of all vibrational levels of the $F^2\Pi$ state. The apparently zero value for the β_4 parameter is consistent with the significant delay between our pump and probe laser, allowing multiple rotations of the excited state CuO molecule prior to single-photon dissociation. Given the myriad of electronic states which correlate with the excited state atomic fragments generated, it would not be surprising if the dissociative state to which excitation takes place were of mixed character. Alternatively, the fact that β_2 takes less than the extreme parallel value ($+2$) may indicate that molecular rotation competes with the actual dissociation process.

The same strong preponderance for dissociation into the $\text{Cu}^* ^2D_{3/2} + \text{O}^* ^1D$ dissociation channel is also observed following

excitation of the CuO $C, D \leftarrow X$ transitions assigned in Fig 3. In each case only a single significant peak is observed in the TKER spectrum. Fig 7 shows the TKER peak position of the observed peak as a function of pump laser wavenumber and includes dissociations out of the F, H, C and D states. The dissociation out

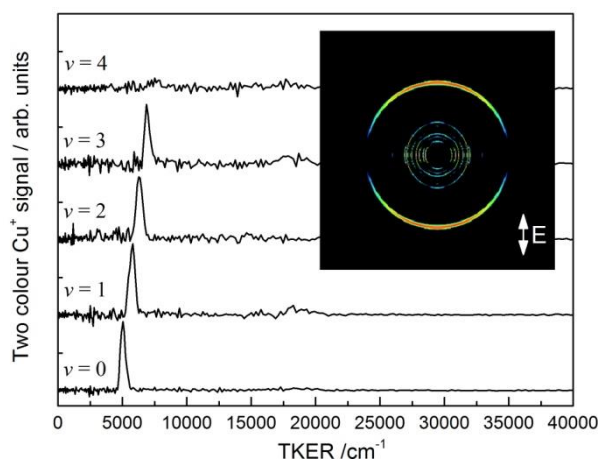


Fig. 6 (colour online) Cu^+ TKER spectra extracted from velocity map images recorded with the visible pump laser resonant with several $\text{CuO } F^2\Pi(v) \leftarrow X^2\Pi(v=0)$ transitions. (inset) VMI image recorded in the Cu^+ mass channel following excitation via the $v=2$ level indicating parallel character to the photodissociation. The orientation of the electric vector of the light in the plane of the detector is indicated.

of the $G \leftarrow X$ transition is not included due to accidental resonance with an OPO-only process. The fact that all points in Fig 7 lie on a straight line with slope 1.00 ± 0.01 ($R^2 = 0.998$) confirms that the transitions involved are single photon in the visible laser. Furthermore, extrapolation of the line to $\text{TKER} = 0 \text{ cm}^{-1}$ permits a precise determination of the CuO dissociation energy: The fitted line in Fig 7 intersects the abscissa at $16194 \pm 243 \text{ cm}^{-1}$. This wavenumber, plus that of the UV photon (37446 cm^{-1}) would, in theory, lead to threshold dissociation into the channel indicated in eqn (4). Hence

$$53640 \pm 243 \text{ cm}^{-1} = D_0(\text{CuO}) + E(\text{Cu}^* {}^2D_{3/2}) + E(\text{O}^* {}^1D). \quad (5)$$

Since the atomic energy levels are well-known,⁵³ we can determine an experimental dissociation energy for ground state CuO of $D_0(\text{CuO}) = 24527 \pm 243 \text{ cm}^{-1}$ ($3.041 \pm 0.030 \text{ eV}$). This value can be compared with a wide variety of values to be found in the literature. Huber and Herzberg quote 2.79 eV for $D_0(\text{CuO})$ from early mass spectrometric determinations⁶¹ whilst Pedley and Marshall give $2.75 \pm 0.22 \text{ eV}$.⁶² Vinckier *et al.* observed that the reaction of Cu with nitrous oxide was thermoneutral over a significant temperature range implying $D_0(\text{CuO}) \approx D_0(\text{ON-O}) = 3.116 \pm 0.008 \text{ eV}$.⁶³ More recently, however, guided ion beam studies Cu^+ with N_2O have yielded a value of $2.94 \pm 0.12 \text{ eV}$ for the dissociation energy of neutral CuO.⁶⁰

Ferraro *et al.*³⁸ have reviewed the various computational studies of CuO and values for D_0 vary from $2.63 - 3.35 \text{ eV}$ depending on the method (and, in the case of DFT, the exchange correlation functional) used. CuO (and CuO^+) has previously been used to illustrate the importance of multiconfigurational wavefunctions in coupled cluster methods which at the CCSD(T) level yields results for D_0 of 2.66 eV ⁶⁴ and 2.78 eV .³⁸

The VMI images shown inset in Fig 7 illustrate the change from predominantly parallel character for dissociation from the $D^2\Delta_{5/2}$ to perpendicular for excitation out of (both spin-orbit components of) the $C^2\Pi$ state.

The ionization energies of Cu and CuO are well known^{51, 55}

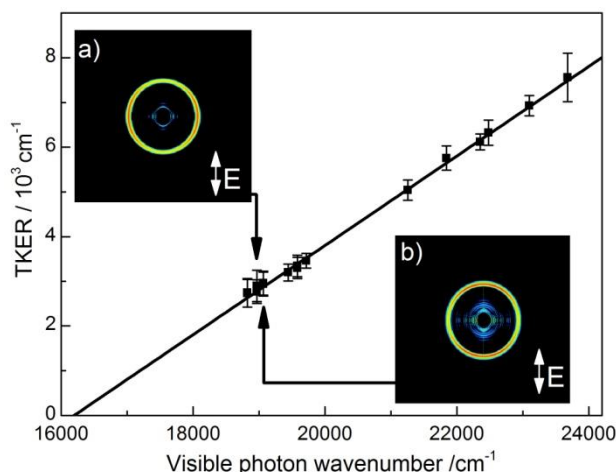
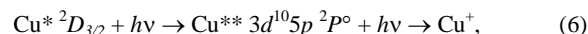


Fig. 7 (colour online) Determination of the CuO $X^1\Sigma$ ground state dissociation energy, D_0 by extrapolation from the peaks identified as corresponding to the $\text{Cu}^* ({}^2D_{3/2}) + \text{O}^* ({}^1D_2)$ channel in the TKER spectra observed following UV photodissociation of the CuO C, D, F and H states. (inset) VMI images recorded via a) the $C^2\Pi_{1/2}(v=0)$ level and b) the $D^2\Delta_{5/2}(v=0)$ level illustrating a change in symmetry.

and as the ground states of CuO and CuO^+ correlate with ground state atomic fragments, we can use our determination of D_0 for CuO to derive the dissociation energy of CuO^+ of $1.36 \pm 0.04 \text{ eV}$. This is in excellent agreement with the guided ion beam CID study of Rodgers *et al.* ($1.35 \pm 0.12 \text{ eV}$)⁶⁰ and somewhat lower than the 1.62 eV from Fisher *et al.*⁶⁵

The dissociation energies derived above are entirely predicated upon our correct assignment of the dissociation channel observed as that given in eqn (4). In order to test this assignment, we have performed “double resonance” studies in which the UV laser was tuned to a nearby resonant 1+1 ionization scheme for the $\text{Cu}^* {}^2D_{3/2}$ state:

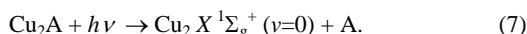


at 36138 cm^{-1} (276.7 nm). Although formally a two electron process this transition is intense in the spectrum of the Cu atom.⁶⁶ When the UV laser is tuned into resonance with this transition, all TKER peaks assigned to the process in eqn (4) are significantly enhanced reflecting an increase in the efficiency in the ionization step eqn (6). This confirms the production of the $\text{Cu}^* {}^2D_{3/2}$ state in the dissociation and, given the scarcity of O atom co-fragment quantum states, this assignment is secure.

3.3 UV photodissociation of larger species

With the UV laser resonant with the $\text{Cu}_2 J \leftarrow X(v=0)$ transitions VMI images were also recorded in the ${}^{63}\text{Cu}_2^+$ mass channel. The signal in this channel is dominated by the Cu_2 R2PI process which gives rise to an intense “on-axis” (*i.e.*, zero kinetic energy release) contribution to the signal. However, in addition, a clear ring is also observed in the VMI images at $\text{KER} \approx 705 \pm 75 \text{ cm}^{-1}$. This clearly indicates the photofragmentation of some larger

species (Cu_2A) in the cluster beam generating $\text{Cu}_2 X^1\Sigma_g^+ (v=0)$:



The image recorded in the Cu_2^+ channel is shown inset in the lower part of Fig 8 along with the kinetic energy release s distribution. This ring, which indicates a weakly perpendicular

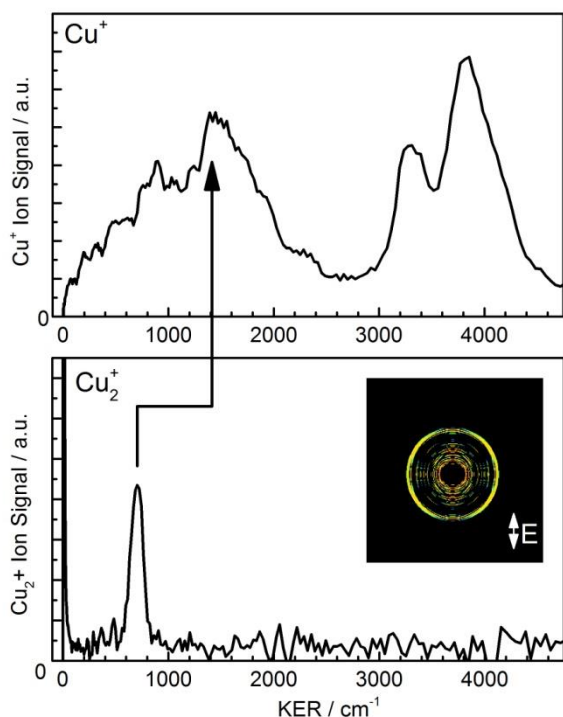


Fig. 8 (colour online) KER spectra recorded gating $^{63}\text{Cu}^+$ (upper) and $^{63}\text{Cu}_2^+$ (lower) ion signals in one colour (UV-only) experiments resonant with the $\text{Cu}_2 J(v=0) \leftarrow X(v=0)$ transition at 37446 cm^{-1} . The presence of a ring in the lower spectrum (see image inset) indicates photodissociation of a larger species than the dimer. In the image the intense central spot due to $\text{Cu}_2 X(v=0)$ in the beam has been removed for clarity. The arrow indicates the expected Cu^+ KER commensurate with the peak in the Cu_2^+ distribution assuming fragmentation of the Cu_3 trimer.

transition, is not present when the laser is off resonance and ionization / detection of Cu_2 is markedly less efficient. The most likely candidate for the fragment A is another Cu atom (*i.e.*, photodissociation of the Cu_3 trimer) and the arrow in Fig 8 indicates the KER in the Cu^+ channel which would be commensurate with this ($\text{KER}(\text{Cu}^+) = 2 \times \text{KER}(\text{Cu}_2^+)$) and satisfy momentum conservation. As discussed previously, this is a congested region in the Cu^+ KER spectrum and although a feature is apparent around 1400 cm^{-1} , this is the region in which we expect Cu atom products following dissociative autoionization out of the $\text{Cu}_2 J$ state. Nevertheless, we proceed under the assumption that this is trimer photodissociation which has been observed previously in the visible using ion depletion⁶⁷ and inert gas tagging.^{68, 69} Previous estimates of the Cu_3 ground state dissociation energy range from $0.75 \pm 0.23 \text{ eV}$ ²² ($0.73 \pm 0.2 \text{ eV}$)²³ derived from CID measurements of Cu_3^+ (yielding $\text{Cu}^+ + \text{Cu}_2$) to $1.08 \pm 0.19 \text{ eV}$.¹ Excitation at 37446 cm^{-1} places us well above this threshold but below the ionization energy of Cu_3 of $5.78 \pm 0.20 \text{ eV}$.⁴² Given that we are selectively ionizing the $\text{Cu}_2 X(v=0)$

state, any excess energy must appear in excited Cu^* fragment. At the one-photon level, production of $\text{Cu } ^2S$, 2D and 2P are energetically possible but only production of 2P states is consistent with low TKER of *ca.* $2115 \pm 170 \text{ cm}^{-1}$ observed. Combining this with the equivalent spectra recorded with the probe laser resonant with the $\text{Cu}_2 J(v=1) \leftarrow X$, this assignment implies a Cu_3 dissociation energy of $0.605 \pm 0.030 \text{ eV}$.

Summary and conclusions

We report a combined spectroscopic / velocity map imaging study of $^{63}\text{Cu}_2$ and ^{63}CuO generated by laser ablation. Spectroscopic tagging is essential due to the lack of mass selectivity within the cluster beam and the unknown cluster size and composition distribution.

One-colour UV excitation of $^{63}\text{Cu}_2$ resonant with the $J - X$ transition results in a complex bimodal structure to the total kinetic energy release spectrum. The spectrum has been interpreted, with the help of the R2PI spectrum recorded *via* the same states, as arising from a combination of i) one-photon dissociation of the $\text{Cu}_2^+ ^2\Pi$ excited state cation and ii) fragmentation of highly excited Cu_2^{**} states above the ionization threshold. Dissociative autoionization of the same Cu_2^{**} states were used to account for the $\text{Cu}_2^+ ^2\Sigma_g^+$ vibrational state distribution observed in the R2PI spectrum. This assignment permits determination of the Cu_2^+ dissociation energy as $D_0(\text{Cu}_2^+, X^2\Sigma_g^+)$ of $1.713 \pm 0.025 \text{ eV}$ which is slightly lower than values derived from extrapolation of fluorescence bands but agrees with recent CID data.

Resonant two-colour excitation of ^{63}CuO via the C, D, F, H states has been used to explore the photodissociation of ^{63}CuO . The resulting VMI images are remarkably simple, exhibiting a single peak in the TKER range $0 - 40000 \text{ cm}^{-1}$ accessible. This dissociation channel is identified as correlating with $\text{Cu } ^2D_{3/2} + \text{O } ^1D$, an assignment confirmed by resonant ionization of the $\text{Cu } ^2D_{3/2}$ state. Extrapolation of the TKER observed following excitation through all excited states leads to a value for the dissociation energy, $D_0(\text{CuO})$ of $3.041 \pm 0.030 \text{ eV}$. This represents a significant refinement over previous measurements.

In UV-only experiments, when the $\text{Cu}_2 J(v) - X$ transitions are excited and Cu_2 ionization is thus efficient, a distinct low KER ring ($\sim 700 \text{ cm}^{-1}$) is observed in $^{63}\text{Cu}_2^+$ signal images. This ring must arise from photofragmentation of larger cluster species, possibly Cu_3 . Such an assignment could only be consistent with production of $\text{Cu}^* ^2P$ states and a Cu_3 dissociation energy of $0.605 \pm 0.030 \text{ eV}$. Additional work, however, remains to be done to confirm this assignment.

Acknowledgements

SRM is grateful to the EPSRC for grant EP/C012070/1 under which the VMI instrument was constructed. ISP and ACH are further grateful to the EPSRC for their studentships. AK acknowledges the Royal Society for his Newton Research Fellowship.

Notes and references

Department of Chemistry,
University of Oxford,

1. M. D. Morse, *Chem. Rev.*, 1986, **86**, 1049-1109.
2. W. Weltner and R. J. Vanzee, *Annu. Rev. Phys. Chem.*, 1984, **35**, 291-327.
3. G. A. Bishea and M. D. Morse, *J. Chem. Phys.*, 1991, **95**, 5646-5659.
4. S. Lecoultrre, A. Rydlo, J. Buttet, C. Felix, S. Gilb and W. Harbich, *J. Chem. Phys.*, 2011, **134**, 184504.
5. J. J. Zhao, X. S. Chen and G. G. Wang, *Phys. Lett. A*, 1994, **189**, 223-226.
6. X. Wang, X. Wan, H. Zhou, S. Takami, M. Kubo and A. Miyamoto, *J. Mol. Struct. (Theochem)*, 2002, **579**, 221-227.
7. J. C. Idrobo, W. Walkosz, S. F. Yip, S. Ogut, J. Wang and J. Jellinek, *Phys. Rev. B*, 2007, **76**, 12.
8. P. Joyes and M. Leleyter, *J. Phys. B-At. Mol. Opt. Phys.*, 1973, **6**, 150-154.
9. R. Hatz, M. Korpinen, V. Hanninen and L. Halonen, *J. Phys. Chem. A*, 2012, **116**, 11685-11693.
10. D. E. Powers, S. G. Hansen, M. E. Geusic, A. C. Puiiu, J. B. Hopkins, T. G. Dietz, M. A. Duncan, P. R. R. Langridgesmith and R. E. Smalley, *J. Phys. Chem.*, 1982, **86**, 2556-2560.
11. D. E. Powers, S. G. Hansen, M. E. Geusic, D. L. Michalopoulos and R. E. Smalley, *J. Chem. Phys.*, 1983, **78**, 2866-2881.
12. M. D. Morse, J. B. Hopkins, P. R. R. Langridgesmith and R. E. Smalley, *J. Chem. Phys.*, 1983, **79**, 5316-5328.
13. C. L. Pettiette, S. H. Yang, M. J. Craycraft, J. Conceicao, R. T. Laaksonen, O. Cheshnovsky and R. E. Smalley, *J. Chem. Phys.*, 1988, **88**, 5377-5382.
14. J. L. Gole, J. H. English and V. E. Bondybey, *J. Phys. Chem.*, 1982, **86**, 2560-2563.
15. R. H. Page and C. S. Gudeman, *J. Chem. Phys.*, 1991, **94**, 39-51.
16. E. A. Rohlfing and J. J. Valentini, *J. Chem. Phys.*, 1986, **84**, 6560-6566.
17. T. Okazaki and Y. Ando, *Mol. Phys.*, 2000, **98**, 447-452.
18. R. S. Ram, C. N. Jarman and P. F. Bernath, *J. Mol. Spectrosc.*, 1992, **156**, 468-486.
19. M. Doverstal, B. Lindgren, U. Sassenberg and H. Yu, *Chem. Phys. Lett.*, 1992, **192**, 283-288.
20. A. D. Sappey, J. E. Harrington and J. C. Weisshaar, *J. Chem. Phys.*, 1988, **88**, 5243-5245.
21. A. D. Sappey, J. E. Harrington and J. C. Weisshaar, *J. Chem. Phys.*, 1989, **91**, 3854-3868.
22. O. Ingolfsson, U. Busolt and K. Sugawara, *J. Chem. Phys.*, 2000, **112**, 4613-4620.
23. S. Kruckeberg, L. Schweikhard, J. Ziegler, G. Dietrich, K. Lutzenkirchen and C. Walther, *J. Chem. Phys.*, 2001, **114**, 2955-2962.
24. E. Miyoshi, H. Tatewaki and T. Nakamura, *Int. J. Quantum Chem*, 1983, **23**, 1201-1207.
25. S. Lecoultrre, A. Rydlo, C. Felix, J. Buttet, S. Gilb and W. Harbich, *J. Chem. Phys.*, 2011, **134**.
26. R. L. Lieberman and A. C. Rosenzweig, *Nature*, 2005, **434**, 177-182.
27. A. J. Merer, *Annu. Rev. Phys. Chem.*, 1989, **40**, 407-438.
28. J. F. Harrison, *Chem. Rev.*, 2000, **100**, 679-716.
29. Y. Gong, M. Zhou and L. Andrews, *Chem. Rev.*, 2009, **109**, 6765-6808.
30. O. Appelblad, A. Lagerqvist and I. Renhorn, *Phys. Scr.*, 1980, **22**, 603-608.
31. J. Schamps, B. Pinchemel, Y. Lefebvre and G. Raseev, *J. Mol. Spectrosc.*, 1983, **101**, 344-357.
32. T. C. Steimle, D. F. Nachman and D. A. Fletcher, *J. Chem. Phys.*, 1987, **87**, 5670-5673.
33. T. C. Steimle, W. L. Chang and D. F. Nachman, *Chem. Phys. Lett.*, 1988, **153**, 534-538.
34. M. C. L. Gerry, A. J. Merer, U. Sassenberg and T. C. Steimle, *J. Chem. Phys.*, 1987, **86**, 4754-4761.
35. M. L. Polak, M. K. Gilles, J. Ho and W. C. Lineberger, *J. Phys. Chem.*, 1991, **95**, 3460-3463.
36. H. B. Wu, S. R. Desai and L. S. Wang, *J. Phys. Chem. A*, 1997, **101**, 2103-2111.
37. S. Midda, N. C. Bera, I. Bhattacharyya and A. K. Das, *J. Mol. Struct. (Theochem)*, 2006, **761**, 17-20.
38. L. F. A. Ferrao, O. Roberto-Neto and F. B. C. Machado, *Int. J. Quantum Chem*, 2008, **108**, 2512-2522.
39. A. Eppink and D. H. Parker, *Rev. Sci. Instrum.*, 1997, **68**, 3477-3484.
40. M. N. R. Ashfold, N. H. Nahler, A. J. Orr-Ewing, O. P. J. Vieuxmaire, R. L. Toomes, T. N. Kitsopoulos, I. A. Garcia, D. A. Chestakov, S. M. Wu and D. H. Parker, *Phys. Chem. Chem. Phys.*, 2006, **8**, 26-53.
41. Y. Matsuda, D. N. Shin and E. R. Bernstein, *J. Chem. Phys.*, 2004, **120**, 4165-4171.
42. M. B. Knickelbein, *Chem. Phys. Lett.*, 1992, **192**, 129-134.
43. G. Alameddine, J. Hunter, D. Cameron and M. M. Kappes, *Chem. Phys. Lett.*, 1992, **192**, 122-128.
44. W. S. Hopkins, S. M. Hamilton, P. D. McNaughton and S. R. Mackenzie, *Chem. Phys. Lett.*, 2009, **483**, 10-15.
45. W. S. Hopkins, A. P. Woodham, R. J. Plowright, T. G. Wright and S. R. Mackenzie, *J. Chem. Phys.*, 2010, **132**, 214303.
46. W. S. Hopkins, A. P. Woodham, R. J. Plowright, T. G. Wright and S. R. Mackenzie, *J. Chem. Phys.*, 2011, **134**, 094311.
47. W. S. Hopkins and S. R. Mackenzie, *J. Chem. Phys.*, 2011, **135**, 081104.
48. W. S. Hopkins and S. R. Mackenzie, *Mol. Phys.*, 2012, **110**, 2465-2475.
49. W. S. Hopkins, A. P. Woodham, N. M. Tonge, A. M. Ellis and S. R. Mackenzie, *J. Phys. Chem. Lett.*, 2011, **2**, 257-261.
50. M. Reid and S. P. K. Koehler, *Rev. Sci. Instrum.*, 2013, **84**.
51. K. B. MacAdam, S. F. Dyubko, V. A. Efremov, V. G. Gerasimov and A. S. Kutsenko, *J. Phys. B-At. Mol. Opt. Phys.*, 2009, **42**.
52. K. Hilpert and K. A. Gingerich, *Ber. Bunsen-Ges. Phys. Chem.*, 1980, **84**, 739-745.
53. A. Kramida, Y. Ralchenko, J. Reader and a. N. A. Team, National Institute of Standards and Technology, Gaithersburg, MD, (2012), p. Available: <http://physics.nist.gov/asd> [2013].
54. J. G. McCaffrey, R. R. Bennett, M. D. Morse and W. H. Breckenridge, *J. Chem. Phys.*, 1989, **91**, 92-103.
55. R. B. Metz, C. Nicolas, M. Ahmed and S. R. Leone, *J. Chem. Phys.*, 2005, **123**.
56. O. Appelblad and A. Lagerqvist, *J. Mol. Spectrosc.*, 1973, **48**, 607-608.
57. O. Appelblad and A. Lagerqvist, *Phys. Scr.*, 1974, **10**, 307-324.
58. O. Appelblad and A. Lagerqvist, *Phys. Scr.*, 1976, **13**, 275-288.
59. O. Appelblad, A. Lagerqvist, Y. Lefebvre, B. Pinchemel and J. Schamps, *Phys. Scr.*, 1978, **18**, 125-136.
60. M. T. Rodgers, B. Walker and P. B. Armentrout, *Int. J. Mass Spectrom.*, 1999, **182**, 99-120.
61. K. P. Huber and G. Herzberg, *Molecular Spectra and Molecular Structure, IV Constants of Diatomic Molecules*, Krieger, Von Nostrand, New York, 1979.
62. J. B. Pedley and E. M. Marshall, *J. Phys. Chem. Ref. Data*, 1983, **12**, 967-1031.
63. C. Vinckier, T. Verhaeghe and I. Vanhees, *J. Chem. Soc.-Faraday Trans.*, 1994, **90**, 2003-2007.
64. C. W. Bauschlicher and P. Maitre, *Theoretica Chimica Acta*, 1995, **90**, 189-203.
65. E. R. Fisher, J. L. Elkind, D. E. Clemmer, R. Georgiadis, S. K. Loh, N. Aristov, L. S. Sunderlin and P. B. Armentrout, *J. Chem. Phys.*, 1990, **93**, 2676-2691.
66. A. G. Shenstone, *Phil. Trans. Roy. Soc.*, 1948, **241**, 297-322.
67. M. F. Jarrold and K. M. Cregan, *Int. J. Mass Spectrom. Ion Processes*, 1990, **102**, 161-181.
68. M. B. Knickelbein, *J. Chem. Phys.*, 1994, **100**, 2388-2390.
69. M. B. Knickelbein, *J. Chem. Phys.*, 1994, **100**, 4729-4737.